UNIWERSYTET TECHNOLOGICZNO-PRZYRODNICZY
IM. JANA I JĘDRZEJA ŚNIADECKICH W BYDGOSZCZY
ZESZYTY NAUKOWE NR 253
TELEKOMUNIKACJA I ELEKTRONIKA 12 (2009), 21-42

SECOND AND HIGHER ORDER WHITENING IMAGE IN RECONSTRUCTION

Nirmal K. Bose[1], Umamahesh Srinivas[1], R. Lee Culver[2]

[1] Department of Electrical Engineering, The Pennsylvania State University
University Park, PA 16802, USA e-mail: bkn@engr.psu.deu

[2] Applied Research Laboratory, The Pennsylvania State University
PO Box 30, State College Pa 16804, USA

Abstract

In natural vision, the information in the natural environment tends to be acquired with minimum redundancy for subsequent handling akin to the technical problems and solutions encountered during the direct or indirect acquisition of compressed or decorrelated (whitened) multidimensional data, their transmission and processing. Considerable challenges are faced when the restrictions of Gaussianity in the signal and noise distributions, and linearity in processing are lifted. We improve recent results in vision research on the concept of higher order whitening of higher order statistics (HOS) based data. This is achieved by modifying the design of the filter and its inverse so that the processed image is of better quality than what is possible by direct implementation of a related scheme. Besides the modified higher order whitener and its complete analysis, the restriction of rotational symmetry in the power spectrum is eliminated in the two-dimensional derivation.

Keywords: whitening, higher-order whitening, power law for images.

1 Motivation

Whitening, in the traditional sense as originally used in filtering, prediction and smoothing of stationary random processes, orthogonalizes the data samples. In communications, such orthogonalization allows the detection algorithm to operate on each output sample independently. In [1], SNR maximization is the main scheme for improving the bit error probability. The difference between the receiver proposed there and conventional ones lies in the presence of a noise-whitening filter. A whitening filter prior to demodulation and smoothing improves the amplitude estimate. The concept of whitening is also widely used in models for signal processing tasks in the retina [2] to achieve a redundancy-reduced representation of

the original input signal. This reduction of second-order correlation is desirable for subsequent processing. The increasing thrust towards higher order statistics (HOS) based signal, data, and information processing embracing non-Gaussianity, non-stationarity and non-linear processing, necessitates removal of redundancies by higher order whitening.

The statistics of the noise affecting real channels significantly deviate from those corresponding to the Gaussian model. Non-Gaussian disturbances are commonly encountered in indoor environments, such as offices, hospitals, and factories as well as in underwater communications applications. If the disturbance is Gaussian and the fading amplitude is Rayleigh-distributed, then the structure of the optimum receiver is a bank of estimator-correlators, possibly preceded by a linear, whitening filter for handling the noise correlation. Receivers designed under the Gaussian noise assumption exhibit dramatic performance degradations in the presence of non-Gaussian impulsive noise. Therefore, attention has been directed (see [3] and [4]) toward the development of non-Gaussian noise models and the design of optimized detection structures that are able to operate in such hostile environments. Buzzi, Conti and Lops [5] modeled the noise as the product of two independent processes, namely, a complex-valued Gaussian process and a real nonnegative one, to account for the fluctuations of the noise source. The noise correlation was accounted for by a whitening linear filter, as for the case of Gaussian noise. Their structure consists of two parallel blocks, namely, an estimator of the short-term PSD plus a bank of estimators correlators, keyed to the estimated PSD of the disturbance. In the non-white noise case, the spectral shape of the noise needs to be estimated and "divided out" of the spectrum. That is, a "prewhitening filter" needs to be constructed and applied to the data so that the noise is whitened. Then the previous case can be applied.

2 Introduction to Second and Higher Order Whitening

Whitening, basically, decorrelates a signal or image by removing statistical redundancies exhibited in the second order statistics of, say, a zero-mean wide-sense stationary random process. A natural image or a sequence of images has considerable spatial as well as temporal (in the case of image sequences) correlation whose removal calls for whitening by linear filtering. In a non-stationary image, higher order correlations that remain require nonlinear methods for their removal based on procedures, referred to as higher order whitening, applied to statistical image models. Crucial in such modeling is the notion of scale-invariance, which refers to an image description that remains fixed with change of image-scale. Scale-invariance is a form of self-similarity, stochastically, a property manifested in a fractal, approximated by objects ubiquitous in nature, like coastlines, clouds, and snow flakes, among many other occurrences in nature.

Wide-sense stationary (WSS) assumption is basic to Wiener filtering and smooth-

ing theory while the popularity of the Gaussian distribution is due to various nice properties it embodies. Images and sequences of images may neither be stationary nor Gaussian and may exhibit highly non-Gaussian statistical behavior. Whitening of Gaussian signals is possible with principal component analysis (PCA) and, in this case, decorrelation is equivalent to statistical independence. Subsequently, independent component analysis (ICA) was developed for handling non-Gaussian sources especially in the problem of blind source separation. ICA methods, however, do not yield statistically independent outputs in case of model inaccuracy and the assumption on the model is also confined, for the most part, to a linear mixture of independent sources whose number also has to be estimated [6].

In the case of a non-Gaussian source vector, when decorrelation does not imply statistical independence, ICA separates a signal (with not more than one Gaussian component) into additive subcomponents subject to the assumption of mutual statistical independence of the non-Gaussian source signals. Most ICA methods are not able to extract the actual number (or order) of source signals, nor the signs or the scales of the sources. Furthermore, ICA is restricted to source vectors $\mathbf{y} = P\mathbf{x}$, where P is a rectangular matrix multiplying the vector $\mathbf{x}$ whose components are assumed to be statistically independent. A decomposition applicable to any matrix, square or rectangular, is the singular value decomposition (SVD),

$$P = USV^T,$$

where U and V are orthogonal matrices and S is the diagonal matrix of singular values. In the case when the singular values are all positive (in general, they are nonnegative) and S is square, $S^{-1/2}$ exists and $S^{-1/2}U^T$ is a whitening transformation (like in PCA) and V is found by minimizing the negentropy.

Typical algorithms for ICA use centering, whitening and dimensionality reduction as preprocessing steps in order to simplify and reduce the complexity of the problem for the actual iterative algorithm. Whitening ensures that all dimensions are treated equally a priori before the algorithm is run. Algorithms for ICA include infomax, FastICA and JADE, but there are many others also. In [7] the SWM (support width measure) contrast is used to solve the ICA problem involving correlated images.This approach is motivated by the unsatisfying results of JADE and FastICA for the same problem, when no other preprocessing than whitening like filtering is used. Its main advantages are its theoretical contrast convexity for bounded sources, its geometrical interpretation and its simplicity. The Probabilistic Independent Component Analysis model is aimed at solving the problem of overfitting in classical ICA. Support vector machines (SVMs) are a set of related supervised learning methods used for classification and regression. They belong to a family of generalized linear classifiers. They can also be considered a special case of Tikhonov regularization. A special property of SVMs is that they simultaneously minimize the empirical classification error and maximize the geometric margin; hence they are also known as maximum margin classifiers.

3 Power Law and Statistical Modeling of Image Databases

Knowledge of the statistical properties of natural images is important in many diverse fields of research. For example, physiologists can test their theories of evolutionary optimization of vision against the measured properties of the environment. At the other end, computer scientists can use the measured statistics to create convincing synthetic environments for the film industry. The class of natural images is receiving attention in image databases used for vision modeling research. These images are sufficiently homogeneous so that a statistical representation model may be constructed for use in compression, denoising, deblurring and also, in the future, for superresolution. Representations using Fourier bases, Gabor bases, wavelet bases and their various ramifications have been extensively used. However, instead of fixed bases, serious attention is needed for generating data driven bases for manipulation and transformation of the data for various tasks (like cognition in the human sensory system). Relatively meagre attention has been directed to research with this type of massive volumetric data. At present, such research thrust is highly computer software (and hardware) driven but more coupling with analytical machineries is needed.

3.1 1-D Analysis

Balboa et al [8] derived results for the power spectra in 1-D by assuming a cut to consist of M independent regions of constant intensity such that the intensity profile of the j-th region is:

$$I_j(x) = \begin{cases} \tilde{I}_j, & x \in [x_j, x_{j+1}] \\ 0, & \text{otherwise.} \end{cases}$$

Here, the $\tilde{I}_j$'s are positive constants and the x_j's are chosen suitably to divide the cut into constant intensity regions. The 1-D cut $I(x)$ can now be represented as

$$I(x) = \sum_{j=1}^{M} I_j(x),$$

whose Fourier transform is

$$\hat{I}(\omega) = \frac{j}{\omega} \sum_{j=1}^{M} \tilde{I}_j (e^{-j\omega x_{j+1}} - e^{-j\omega x_j}),$$

where $\omega = 2\pi f$ and f is the spatial frequency. The power spectrum of $I(x)$ is

$$|\hat{I}(\omega)|^2 = \frac{1}{\omega^2} \left| \sum_{j=1}^{M} \tilde{I}_j (e^{-j\omega x_{j+1}} - e^{-j\omega x_j}) \right|^2.$$

The observation made in [8] is that as spatial frequency increases, the summation term in the last equation varies but the envelope falls as $1/\omega^2$. Further, at very

low spatial frequencies corresponding to $\omega < 1/(x_{J+1} - x_J)$, where $(x_{j+1} - x_j)$ is maximum at $j = J$, a Taylor series expansion (around $x = x_j$) leads to the approximation

$$|\hat{I}(\omega)|^2 \simeq \left| \sum_{j=1}^{M} \tilde{I}_j (x_{j+1} - x_j)(e^{-j\omega x_j}) \right|^2,$$

which reveals that the envelope is approximately constant at very low frequencies.

3.2 2-D Analysis

The reasoning presented above is generalized to a 2-D image $I(x, y)$. Again, the image is treated as continuous rather than as a set of discrete pixels. The 2-D Fourier transform of $I(x, y)$ is

$$\hat{I}(\omega_x, \omega_y) = \int_{-\infty}^{\infty} \int_{-\infty}^{\infty} I(x, y) e^{-j\omega_x x} e^{-j\omega_y y} dx \; dy,$$

where ω_x and ω_y are the bivariate independent angular frequency components. Actually, the integrand is non-zero only over the finite support of the image in 2-D space.

The Fourier transform along the ω_x-axis at $\omega_y = 0$ is

$$\hat{I}(\omega_x, 0) = \int_{-\infty}^{\infty} \left(\int_{-\infty}^{\infty} I(x, y) e^{-j\omega_x x} dx \right) dy.$$

The integral within parentheses is evaluated for an arbitrary but fixed y for equivalence to a 1-D cut analysis. Now let $I(x, y) = \sum_{j=1}^{M(y)} I_j(x, y)$, where

$$I_j(x, y) = \begin{cases} \tilde{I}_j(y), & x \in [x_j, x_{j+1}] \\ 0, & \text{otherwise.} \end{cases}$$

Note that $\tilde{I}_j(y)$ is a constant for the specified range of x at a particular value of y. It however may vary with y and this dependence on y is expressed as $\tilde{I}_j(y)$. Also, the number of constant-intensity regions varies with y and this explains the dependence of M on y in the summation. Proceeding parallel to the 1-D case discussed above leads to the modified results

$$\hat{I}(\omega_x, 0) = \frac{j}{\omega_x} \int_{-\infty}^{\infty} \sum_{j=1}^{M(y)} \tilde{I}_j(y)(e^{-j\omega x_{j+1}} - e^{-j\omega x_j}) dy, \tag{1}$$

$$|\hat{I}(\omega_x, 0)|^2 = \frac{1}{{\omega_x}^2} \left| \int_{-\infty}^{\infty} \sum_{j=1}^{M(y)} \tilde{I}_j(y)(e^{-j\omega x_{j+1}} - e^{-j\omega x_j}) dy \right|^2. \tag{2}$$

The x_{j+1} and x_j implicitly correspond to (x_{j+1}, y) and (x_j, y), respectively. Clearly, the envelope of the power spectrum falls as $1/{\omega_x}^2$ even though the integral term

may fluctuate. A similar analysis for the case $\omega_x = 0$ leads to the result that the power spectrum falls as $1/{\omega_y}^2$.

The more general case of 2-D Fourier transform is now considered. Extending the idea of constant-intensity regions to two dimensions, the image is divided into rectangular patches, each having pixels of the same intensity values. The image is divided into MN rectangles using $M+1$ vertical lines $x = x_j, j = 1, 2, \ldots, M+1$, and $N+1$ horizontal lines $y = y_k, k = 1, 2, \ldots, N+1$. The rectangle bounded by the four lines $x = x_j$, $x = x_{j+1}$, $y = y_k$ and $y = y_{k+1}$ is assumed to have constant intensity $\tilde{I}_{jk}$.

3.3 Division of the image into rectangular patches

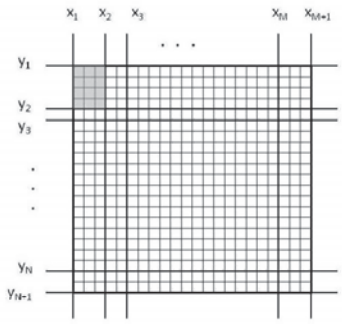

Figure 1: Figure showing the division of the original image into constant-intensity rectangular patches. The shaded region shows one such rectangular patch.

The procedure to divide the image is as follows. Starting from the left vertical boundary of the image (i.e., $x = x_1$), the image is scanned from left to right to check if each column is identical to the column immediately preceding it. The line $x = x_2$ is drawn between adjacent columns L_1 and L_2 where at least one pixel of L_2 differs from the corresponding pixel on the same row in the preceding column L_1. Proceeding thus, all the vertical lines $x = x_2$ to $x = x_M$ are located. Similarly, starting with the upper horizontal image boundary ($y = y_1$), the image is scanned from top to bottom and each horizontal line $y = y_k$ is located between rows where at least one pixel differs from the corresponding pixel on the same column in the preceding row. Figure 1 schematically shows the division of the original image.

Some observations regarding the image division are discussed next. This method does not divide the image into the largest possible regions of constant intensity. The particular method discussed above divides the image based on a uniform grid which simplifies mathematical calculations, and it is likely that more than one region may have identical intensity values. For a white noise image, the rectangles will be of size 1 pixel, since the pixel intensity values are completely independent

of other pixels. Balboa et al [8] derived the result for the 1-D case based on the assumption that images consist of individual constant-intensity patches. This assumption is not valid in the type of 2-D generalization considered here.

3.4 2-D Fourier analysis: general case

Let the intensity profile of the image be described by:

$$I(x,y) = \sum_{k=1}^{N}\sum_{j=1}^{M} I_{jk}(x,y),$$

where

$$I_{jk}(x,y) = \begin{cases} \tilde{I}_{jk}, & x \in [x_j, x_{j+1}] \text{ and } y \in [y_k, y_{k+1}] \\ 0, & \text{otherwise.} \end{cases}$$

For a specified 2-tuple (j,k), $I_{jk}(x,y)$ denotes a constant intensity rectangular patch and $\tilde{I}_{jk}$ is the value of this constant. Let $\hat{I}_{jk}(\omega_x,\omega_y)$ be the Fourier transform of the patch $I_{jk}(x,y)$. Then, the Fourier transform of $I(x,y)$ is given by:

$$\begin{aligned}
\hat{I}(\omega_x,\omega_y) &= \sum_{k=1}^{N}\sum_{j=1}^{M} \hat{I}_{jk}(\omega_x,\omega_y) \\
&= \sum_{k=1}^{N}\sum_{j=1}^{M} \int_{y_k}^{y_{k+1}} \int_{x_j}^{x_{j+1}} I_{jk}(x,y) e^{-j\omega_x x} e^{-j\omega_y y} dx\ dy \\
&= \sum_{k=1}^{N}\sum_{j=1}^{M} \left\{ \tilde{I}_{jk} \int_{x_j}^{x_{j+1}} e^{-j\omega_x x} dx \int_{y_k}^{y_{k+1}} e^{-j\omega_y y} dy \right\} \\
&= \frac{-1}{\omega_x \omega_y} \sum_{k=1}^{N}\sum_{j=1}^{M} \tilde{I}_{jk} (e^{-j\omega_x x_{j+1}} - e^{-j\omega_x x_j})(e^{-j\omega_y y_{k+1}} - e^{-j\omega_y y_k}).
\end{aligned}$$

Note that $\tilde{I}_{jk}$ is a function of j and k and cannot be moved outside the summation in the last equation. The power spectrum is

$$|\hat{I}(\omega_x,\omega_y)|^2 = \frac{1}{{\omega_x}^2 {\omega_y}^2} \left| \sum_{k=1}^{N}\sum_{j=1}^{M} \tilde{I}_{jk} (e^{-j\omega_x x_{j+1}} - e^{-j\omega_x x_j})(e^{-j\omega_y y_{k+1}} - e^{-j\omega_y y_k}) \right|^2. \tag{3}$$

The term inside the summation on the RHS varies with j and k, but the envelope of the power spectrum falls as $1/({\omega_x}^2 {\omega_y}^2)$. At very low spatial frequencies, $\omega_x < 1/(x_{J+1} - x_J)$, where $(x_{j+1} - x_j)$ is maximum for $j = J$, and $\omega_y < 1/(y_{K+1} - y_K)$, where $(y_{k+1} - y_k)$ is maximum for $k = K$. Then, $e^{-j\omega_x x_{j+1}} \simeq e^{-j\omega_x x_j} - j\omega_x (x_{j+1} - x_j) e^{-j\omega_x x_j}$, and $e^{-j\omega_y y_{k+1}} \simeq e^{-j\omega_y y_k} - j\omega_y (y_{k+1} - y_k) e^{-j\omega_y y_k}$, by Taylor series

expansion (around each 2-tuple ($x = x_j$, $y = y_k$)). So,

$$\begin{aligned} |\hat{I}(\omega_x, \omega_y)|^2 &\simeq \frac{1}{{\omega_x}^2 {\omega_y}^2} \left| \sum_{k=1}^{N} \sum_{j=1}^{M} \tilde{I}_{jk}(-j\omega_x)(x_{j+1} - x_j) e^{-j\omega_x x_j} (-j\omega_y)(y_{k+1} - y_k) e \right. \\ &= \left| \sum_{k=1}^{N} \sum_{j=1}^{M} \tilde{I}_{jk}(x_{j+1} - x_j) e^{-j\omega_x x_j} (y_{k+1} - y_k) e^{-j\omega_y y_k} \right|^2 . \end{aligned}$$

This shows that at very low spatial frequencies, the envelope of the power spectrum is approximately constant with frequency.

4 Observations

To summarize the results, the 2-D power spectra of images fall off as $1/({\omega_x}^2 {\omega_y}^2)$, where ω_x and ω_y are the components in the wavenumber (angular frequency) domain. Along the ω_x-axis, the spectra fall off as $1/{\omega_x}^2$, and as $1/{\omega_y}^2$ along the ω_y-axis. At very low spatial frequencies, the envelope of the spectrum is approximately constant. In [9], the authors provide justification for why the spectrum is flat at very low frequencies.

4.1 Gradients of illumination

The case of gradients of illumination discussed in Balboa [8] for 1-D can be extended to 2-D. The simplest model for expressing gradients (variable-separable case) is:

$$I_{jk}(x, y) = \begin{cases} \tilde{I}_{jk} + \gamma xy, & x \in [x_j, x_{j+1}] \text{ and } y \in [y_k, y_{k+1}] \\ 0, & \text{otherwise} \end{cases}$$

where γ is a constant. Since $I(x, y) = \sum_{k=1}^{N} \sum_{j=1}^{M} I_{jk}(x, y)$, the Fourier transform of $I(x, y)$ is obtained as:

$$\hat{I}(\omega_x, \omega_y) = \sum_{k=1}^{N} \sum_{j=1}^{M} \hat{I}_{jk}(\omega_x, \omega_y),$$

where

$$\begin{aligned} \hat{I}_{jk}(\omega_x, \omega_y) &= \int_{y_k}^{y_{k+1}} \int_{x_j}^{x_{j+1}} (\tilde{I}_{jk} + \gamma xy) e^{-j\omega_x x} e^{-j\omega_y y} dx\, dy \\ &= \tilde{I}_{jk} \int_{x_j}^{x_{j+1}} e^{-j\omega_x x} dx \int_{y_k}^{y_{k+1}} e^{-j\omega_y y} dy + \gamma \int_{x_j}^{x_{j+1}} x e^{-j\omega_x x} dx \int_{y_k}^{y_{k+1}} y \\ &= \frac{-\tilde{I}_{jk}}{\omega_x \omega_y} (e^{-j\omega_x x_{j+1}} - e^{-j\omega_x x_j})(e^{-j\omega_y y_{k+1}} - e^{-j\omega_y y_k}) + I_1, \end{aligned}$$

and I_1 can be simplified using integration by parts as

$$I_1 = \gamma \left\{ \frac{j}{\omega_x}(x_{j+1}e^{-j\omega_x x_{j+1}} - x_j e^{-j\omega_x x_j}) + \frac{1}{\omega_x^2}(e^{-j\omega_x x_{j+1}} - e^{-j\omega_x x_j}) \right\}$$
$$\left\{ \frac{j}{\omega_y}(y_{k+1}e^{-j\omega_y y_{k+1}} - y_k e^{-j\omega_y y_k}) + \frac{1}{\omega_y^2}(e^{-j\omega_y y_{k+1}} - e^{-j\omega_y k_k}) \right\}.$$

Thus, $\hat{I}_{jk}(\omega_x, \omega_y)$ contains a term proportional to $1/(\omega_x^2\omega_y^2)$ and the power spectrum given by $|\hat{I}(\omega_x, \omega_y)|^2 = |\sum_{k=1}^{N}\sum_{j=1}^{M}\hat{I}_{jk}(\omega_x, \omega_y)|^2$ is proportional to $1/(\omega_x^4\omega_y^4)$, which implies a steeper descent than $1/(\omega_x^2\omega_y^2)$. Thus, illumination gradients lead to a steeper descent of the power spectrum in 2-D. Other models to describe the effects of illumination are possible and only the simplest case has been dealt with here.

4.2 Statistical independence

According to Ruderman [10], *statistically independent* regions have random size, location and intensity. The segmentation performed by Ruderman is based on dividing images into largest possible regions of constant intensity and the regions are of various irregular shapes. Consequently, adjacent independent regions in the image are unlikely to have correlation in pixel intensities. In contrast, the image segmentation into rectangular patches explained in this report is based on a uniform rectangular grid of lines. It is possible to have adjacent regions with the same intensity since both regions may in fact belong to the same object. Hence, the rectangular regions may not be statistically independent.

One more point to be noted is that since the power spectrum $|\hat{I}(\omega_x, \omega_y)|^2$ is proportional to $1/(\omega_x^2\omega_y^2)$, points in the wavenumber (angular frequency) domain satisfying $\omega_x\omega_y = c$ where c is some constant, show identical spectrum fall-off behavior. These points lie on a rectangular hyperbola. In comparison, for the rotation-averaged case, the power spectrum $\hat{P}(\omega) \propto 1/\omega^2$ and $\omega = \sqrt{\omega_x^2 + \omega_y^2}$ and the points showing identical fall-off behavior lie on a circle.

5 Higher Order Whitening and De-whitening Filters

This section discusses higher order whitening, in particular the filter described by Gluckman [11]. A second-order whitening filter is first designed to remove correlations between image pixel intensities, as specified by Olshausen [12]. It is established that images have considerable regularity in their second order spatial correlations as measured by the autocorrelation or power spectrum [13]. It has been observed that the orientation-averaged power spectrum $P(f)$ varies with spatial angular frequency f as:

$$P(f) \propto 1/f^2, \tag{4}$$

where $f = \sqrt{f_1^2 + f_2^2}$ and the 2-D frequency response is defined in the (f_1, f_2)-plane. So, it is logical to design a whitening filter whose magnitude of frequency response varies as f so that the whitened image has a 'flat' power spectrum. A crucial assumption in this procedure is that of circular symmetry of the inherently 2-D frequency response in the (f_1, f_2)-plane required for filtering 2-D image data.

After second order whitening, lines and edges, which correspond to higher order correlations, are visible in the whitened image. These correlations can be removed using higher order whitening. In the method discussed in [11], the (second order) whitened image $W(\mathbf{x})$ may be expressed as:

$$W(\mathbf{x}) = g(\mathbf{x}) * I(\mathbf{x}), \tag{5}$$

where $\mathbf{x} \equiv (x_1, x_2)$, $I(\mathbf{x})$ is the original image and $g(\mathbf{x})$ is the second order whitening filter unit impulse response with the property that the magnitude of its Fourier transform, $|\hat{g}(f)|$, is proportional to f. $W(\mathbf{x})$ may assume both positive and negative values. The statistics of second order whitened images are unstable (in the sense of large dynamic range) due to the high kurtosis of pixel intensities and so Gluckman suggests usage of the log magnitude whitened image $L(\mathbf{x}) = log|W(\mathbf{x})|$ for further whitening. He further conjectured, based only on simulations, that $L(\mathbf{x})$ also obeys a power law similar to that in Equation (4) and hence filtering it with the second order whitening filter g produces higher order whitening. The higher order whitened image $H(\mathbf{x})$ is obtained as

$$H(\mathbf{x}) = sgn(W(\mathbf{x}))\ exp\{g(\mathbf{x}) * log|W(\mathbf{x})|\}. \tag{6}$$

This equation characterizes a form of homomorphic filtering. The sgn term represents the $signum$ function. $H(\mathbf{x})$ in (6) assumes both positive and negative values due to the presence of $sgn(W(\mathbf{x}))$. Figure 2 shows the higher order whitening scheme followed in [11].

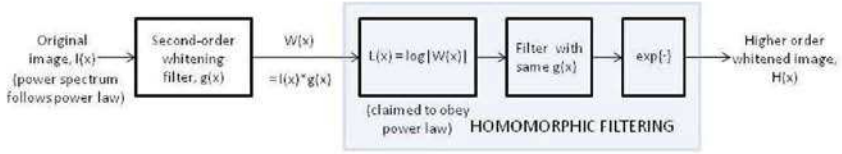

Figure 2: Schematic showing the steps in the higher-order whitening procedure suggested by Gluckman.

A brief analysis of the above higher order filter equation follows. The original image can be recovered from the higher order whitened image by a straightforward inverting procedure described by Equation 10 in reference [11]. The identities $H(\mathbf{x}) = |H(\mathbf{x})|sgn(H(\mathbf{x}))$ and $sgn(H(\mathbf{x}))^2 = 1$ are easily seen to hold. Applying the $signum$ function to both sides of Eq. (6), one gets $sgn(H(\mathbf{x})) = sgn(W(\mathbf{x}))$.

For notational brevity, the explicit functional dependence on the variable $\mathbf{x}$ is dropped. Multiplying both sides of Eq. (6) by $sgn(H)$, one gets

$$\begin{aligned} Hsgn(H) &= sgn(H)sgn(W)\ exp\{g * log|W|\} \\ &= exp\{g * log|W|\}. \end{aligned}$$

But the left hand side of the preceding equation is equal to $|H|$. So, denoting the inverse of the whitening filter unit impulse response g by g^{-1}, it follows that

$$\begin{aligned} |W| &= exp\{g^{-1} * log|H|\} \\ \text{i.e., } W &= sgn(W)\ exp\{g^{-1} * log|H|\}. \end{aligned}$$

Therefore, convolving both sides of Eq. (5) with g^{-1}, substituting the preceding expression for W and noting that $sgn(W) = sgn(H)$, it follows that

$$I(x) = g^{-1} * [sgn(H)\ exp\{g^{-1} * log|H|\}]. \tag{7}$$

Eq. (7) is identical to Eq. 10 in [11]. To get the modified filter proposed here, drop the sgn term in Eq. (6) and then replace the higher order whitening filter H by

$$H_1 = exp\{g * log|W|\}. \tag{8}$$

Noting that H_1 assumes only positive values (since $exp\{g * log|W|\} > 0$), it follows that

$$g * log|W| = log(H_1) = log|H_1|.$$

Following arguments similar to the ones above and inserting the identity $sgn(H_1) \equiv 1$, the counterpart of Eq. (7) becomes

$$I = g^{-1} * [sgn(H_1)\ exp\{g^{-1} * log|H_1|\}]. \tag{9}$$

Equations (7) and (9) are equivalent except that $sgn(H_1) \equiv 1$ in Eq. (9) (because in Eq. (8), $H_1 > 0$ always). It will be found later from simulations that this replacement of H by H_1 improves the overall quality of the reconstructed images after higher order whitening.

6 Simulation results

6.1 Second order whitening based on 2-D power law

Results of simulations to verify the 2-D power law proposed in Equation (3) are presented in this section. A second order whitening filter G is designed in the frequency domain such that:

$$\hat{G}(\omega_x, \omega_y) = \begin{cases} \omega_x\omega_y, & \omega_x \neq 0 \text{ and } \omega_y \neq 0 \\ \omega_x, & \omega_y = 0 \\ \omega_y, & \omega_x = 0. \end{cases}$$

From Eqs. (2) and (3), it can be seen that filtering an image with the above whitening filter leads to an approximately flat spectrum over a significant range of

frequencies. The image power spectrum shows that most of the energy is concentrated in the low spatial frequencies and the spectrum falls off with higher frequencies. The power spectrum of the filter proposed above increases in magnitude with spatial frequencies, resulting in a whitened image with amplified high-frequency noise. To avoid this problem, the whitening filter may be combined with a 2-D lowpass filter and then applied to images. The modified whitening filter, based on a filter proposed by Liao et al in [14], is given by:

$$\hat{G}_1(\omega_x, \omega_y) = \hat{G}(\omega_x, \omega_y) \exp\left\{ -k \left(\frac{\sqrt{\omega_x^2 + \omega_y^2}}{\omega_c} \right)^n \right\}, \tag{10}$$

where k, ω_c and n are parameters which can be suitably varied to achieve a flat spectrum ($k = 1$ in [14]). The exponential term acts as a lowpass filter, and the cut-off frequency is determined by ω_c.

For the set of images considered, the parameter value $\omega_c = 0.05N$, where the input image size is $N \times N$. By suitably choosing the parameters k and n in Equation (10), flat spectra over larger range of frequencies can be obtained. The whitening was performed on different sets of images: natural, mixed and thermal. The natural and mixed scenery visible images have been sourced from the van Hateren database [15], while the thermal images have been sourced from Morris et al [16].

The whitened image obtained in each case reveals that most of the correlations between pixels in the image have been removed. As a means of comparison, the rotation-averaged 1-D power spectra are plotted. Some of the image spectra have distinct streaks along the ω_x and ω_y axes. These streaks may not be sufficiently flattened in the process of whitening. Schaaf and Hateren [17] suggest that one reason for the appearance of such streaks could be that, on average, there are more horizontally and vertically oriented structures in natural images. Langer [18] explains why scaling may fail in individual images, and how the appearance of the streaks is determined by the shape and size of the image window.

The whitening filter is separable and is easily invertible. Accordingly, a 2-D de-whitening filter $\hat{G}^{-1}(\omega_x, \omega_y)$ is designed in the frequency domain as follows:

$$\hat{G}^{-1}(\omega_x, \omega_y) = \begin{cases} 1/(\omega_x \omega_y), & \omega_x \neq 0 \text{ and } \omega_y \neq 0 \\ 1/\omega_x, & \omega_y = 0 \\ 1/\omega_y, & \omega_x = 0. \end{cases} \tag{11}$$

The modified whitening filter in Eq. (10) has an exponential term which also can be incorporated into the de-whitening filter as:

$$\hat{G}_1^{-1}(\omega_x, \omega_y) = \hat{G}^{-1}(\omega_x, \omega_y) \exp\left\{ k \left(\frac{\sqrt{\omega_x^2 + \omega_y^2}}{\omega_c} \right)^\eta \right\}. \tag{12}$$

6.1.1 Natural image - second order whitening and de-whitening using 2-D filter

(a) Original image.

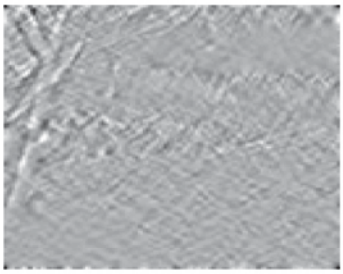

(b) Whitened image using 2-D filter.

(c) Reconstructed image using 2-D de-whitening filter.

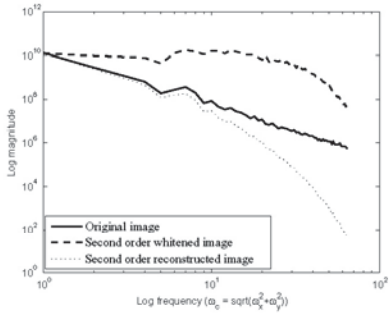

(d) Rotation-averaged power spectra.

(e) Whitened image - Gluckman's filter.

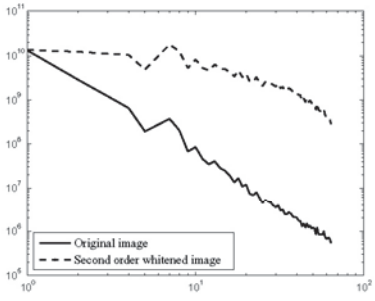

(f) Rotation-averaged power spectra - Gluckman.

Figure 3: Natural image - second order whitening and de-whitening. 2-D filter parameter values used: $k = 0.3, \eta = 1.2$. The 2-D filter used in (b) decorrelates the image better than Gluckman's filter in (e).

6.1.2 Mixed scenery visible image - second order whitening and de-whitening using 2-D filter

(a) Original image.

(b) Whitened image using 2-D filter.

(c) Reconstructed image using 2-D de-whitening filter.

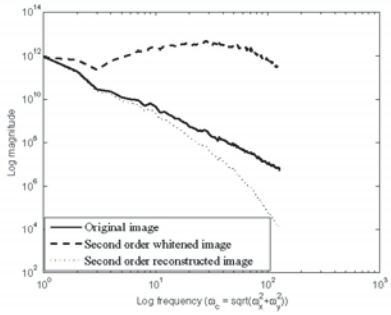

(d) Rotation-averaged power spectra.

(e) Whitened image - Gluckman's filter.

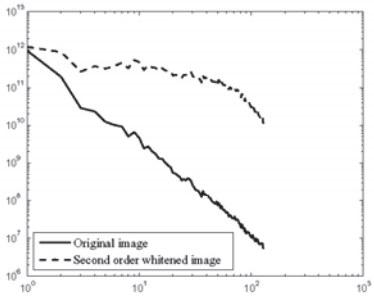

(f) Rotation-averaged power spectra - Gluckman.

Figure 4: Mixed scenery image - second order whitening and de-whitening. 2-D filter parameter values used: $k = 0.4, \eta = 0.9$. The 2-D filter used in (b) decorrelates the image better than Gluckman's filter in (e).

6.1.3 Textured visible image - second order whitening and de-whitening using 2-D filter

(a) Original image.

(b) Whitened image using 2-D filter.

(c) Reconstructed image using 2-D de-whitening filter.

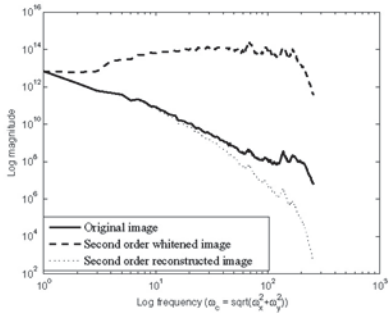

(d) Rotation-averaged power spectra.

(e) Whitened image - Gluckman's filter.

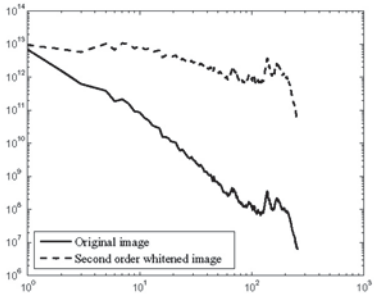

(f) Rotation-averaged power spectra - Gluckman.

Figure 5: Mixed scenery image (highly-textured) - second order whitening and de-whitening. 2-D filter parameter values used: $k = 0.3, \eta = 1.2$. The 2-D filter used in (b) decorrelates the image better than Gluckman's filter in (e).

6.1.4 Thermal image - second order whitening and de-whitening using 2-D filter

(a) Original image.

(b) Whitened image using 2-D filter.

(c) Reconstructed image using 2-D de-whitening filter.

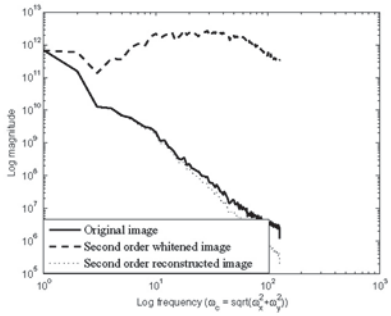

(d) Rotation-averaged power spectra.

(e) Whitened image - Gluckman's filter.

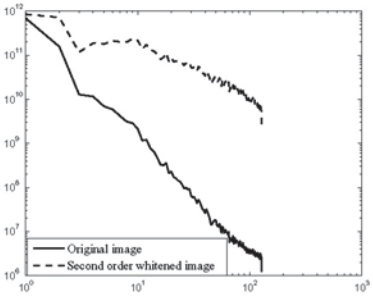

(f) Rotation-averaged power spectra - Gluckman.

Figure 6: Thermal image - second order whitening and de-whitening. 2-D filter parameter values used: $k = 0.1, \eta = 1.0$. The 2-D filter used in (b) decorrelates the image better than Gluckman's filter in (e).

Simulation results from a variety of test image data - natural, mixed scenery, textured, thermal - show that a satisfactory reconstruction of the original image can be obtained by filtering with G^{-1} from Eq. (11) itself. This obviates the need for the additional three parameters k, η and ω_c at the de-whitening side. Exact reconstruction is achieved by using the de-whitening filter specified in Eq. (12).

6.2 Higher order whitening

Higher order whitening is performed on a sample thermal image sourced from Morris et al [16]. The procedure followed is described in Equations (5) and (6). The second order and higher order whitened images are displayed. The reconstructed original image is shown for the two cases: with the signum function in the higher order filter as proposed by Gluckman, and without the signum function as proposed in this paper. Results are shown in Figures 7-9.

Next, the higher order whitening and de-whitening using Gluckman's procedure is repeated using the 2-D whitening filter proposed in this paper. The higher order whitened image and the log power spectra are shown in Figures 10 and 11, respectively.

6.2.1 Thermal image - higher order whitening and de-whitening using Gluckman's procedure

(a) (b)

Figure 7: (a) Original thermal image, (b) Second order whitened image using Gluckman's orientation-averaged whitening procedure.

(a) (b)

Figure 8: (a) Higher order whitened image using Gluckman's higher order whitening procedure, (b) Reconstructed original image (signum term used in higher order whitening, as proposed by Gluckman).

(a) (b)

Figure 9: (a) Higher order whitened image using Gluckman's higher order whitening procedure, (b) Reconstructed original image (signum term not used in higher order whitening, as proposed in this paper).

6.2.2 Thermal image - higher order whitening and de-whitening combining 2-D filter and Gluckman's procedure

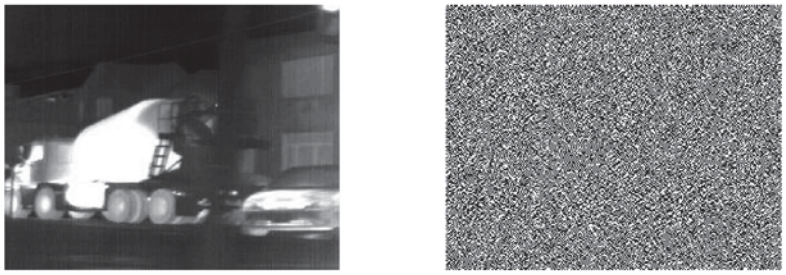

(a) (b)

Figure 10: (a) Original thermal image, (b) Higher order whitened image (decorrelated) using Gluckman's procedure and a 2-D second order whitening filter.

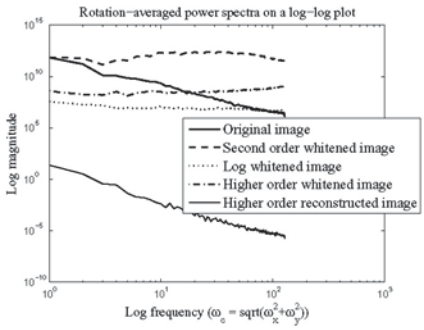

Figure 11: Power spectra plotted as a function of the rotation-averaged frequency for comparison.

7 Conclusions

This paper is concerned with the problems and solutions encountered during the acquisition of compressed multidimensional data, their transmission and processing when the assumptions of Gaussianity in the signal and noise distributions and linearity in processing need not hold simultaneously. While attempting such a generalization one feels the need for more powerful analytical tools with which to develop technical devices to tackle the increasing complexities of the models. For example the fundamental concept of whitening for second order statistics based

signal or data forms the nucleus for generalization to higher order whitening of higher order statistics (HOS) based data, where both the higher order whitening filter and its inverse have nonrational nonlinear input/output descriptions. Their implementations are done by software for the simulated examples in this paper. A modification of the second and higher order whitening filters in [11] is proposed in this paper. It is seen from simulation on infrared images that the visual quality of the reconstructed image is better using the proposed modifications. For example, in Figure 8, black specks are seen in the white regions (corresponding to hotter areas) of the reconstructed image, while the specks are missing in the reconstructed image in Figure 9. This suggests that the sgn factor is not only redundant but also may be harmful in higher order filtering. Also, Gluckman's conjecture that the log magnitude second order whitened image follows the power law in Equation (4) is not necessarily true, as shown by the power spectrum plot in Figure 11, in which the log whitened image spectrum is nearly flat.

The concept of whitening, in turn, has strong links to choice of bases for compressed signal representation, their coding (sparse or otherwise) and reconstruction by constrained optimization using mixed norms. These links are currently under detailed investigation with respect to properties like wavelength diversity as briefly reported here and elsewhere [19] with respect to visible and thermal wavelength images. The results here contribute to the goal for unification of different but related concepts (like whitening and compressed signals) and further development of mathematical (simultaneous matrix diagonalization, simultaneous matrix singular value decomposition, simultaneous matrix polar decomposition) as well as probabilistic descriptions (Gaussian as well as non-Gaussian distributions) for detection, estimation, sampling and processing of signals.

Acknowledgement

The research reported here was conducted under the sponsorship of the National Science Foundation Grant CCF-0429481 and the Office of Naval Research, Undersea Signal Processing, Program Code 321US. Constructive comments by the reviewers are gratefully acknowledged and incorporated in the revised manuscript prior to publication.

Bibliography

[1] A. M. Monk, M. Davis, L. B. Milstein, and C. W. Helstrom, "A noise whitening approach to multiple access noise rejection part I: theory and background," *IEEE Journal on Selected Areas in Communications*, vol. 12, no. 5, June 1994.

[2] J. J. Atick and A. N. Redlich, "What does the retina know about natural scenes?" *Neural Computations*, vol. 4, pp. 196–210, 1992.

[3] S. Buzzi, E. Conte, A. D. Maio, and M. Lops, "Optimum diversity detection over fading dispersive channels with non-Gaussian noise," *IEEE Trans. Signal Process.*, vol. 49, no. 4, pp. 767–776, April 2001.

[4] H.-F. Chen, X.-R. Cao, H.-T. Fang, and J. Zhu, "Nonlinear adaptive blind whitening for MIMO channels," *IEEE Trans. Signal Process.*, vol. 53, no. 8, pp. 2635–2647, August 2005.

[5] S. Buzzi, E. Conte, and M. Lops, "Optimum detection over Rayleigh-fading, dispersive channels, with non-Gaussian noise," *IEEE Trans. Comm.*, vol. 45, no. 9, pp. 1061–1069, September 1997.

[6] A. Hyvärinen, J. Karhunen, and E. Oja, *Independent Component Analysis.* Wiley Interscience, 2001.

[7] F. Vrins and M. Verleysen, "SWM: A class of convex contrasts for source separation," in *Proc. IEEE Int. Conf. Acoust., Speech, and Signal Process.*, Philadelphia, US, 2005.

[8] R. M. Balboa, C. W. Tyler, and N. M. Grzywacz, "Occlusions contribute to scaling in natural images," *Vision Research*, vol. 41, pp. 955–964, 2001.

[9] N. M. Grzywacz, R. M. Balboa, and C. W. Tyler, "A reply to a letter to the editor by Ruderman," *Vision Research*, vol. 42, pp. 2803–2805, 2002.

[10] D. L. Ruderman, "Origins of scaling in natural images," *Vision Research*, vol. 37, no. 23, pp. 3385–3398, 1997.

[11] J. Gluckman, "Higher order whitening of natural images," *Proc. of the IEEE Conference on Computer Vision and Pattern Recognition*, vol. 2, no. 12, pp. 354–360, June 2005.

[12] B. Olshausen. [Online]. Available: http://redwood.berkeley.edu/bruno/npb261b/lab2/lab2.html

[13] D. J. Field, "Relations between the statistics of natural images and the response profiles of cortical cells," *Journal of the Optical Society of America A*, pp. 2379–2394, 1987.

[14] L.-Z. Liao, S.-W. Luo, and M. Tian, "Whitenedfaces recognition with PCA and ICA," *IEEE Signal Processing Letters*, vol. 14, no. 12, pp. 1008–1011, December 2007.

[15] J. H. van Hateren and A. van der Schaaf, "Independent component filters of natural images compared with simple cells in primary visual cortex," *Proc. of the Royal Statistical Society of London (B)*, vol. 265, pp. 359–366, 1998.

[16] N. J. W. Morris, S. Avidan, W. Matusik, and H. Pfister, "Statistics of infrared images," *Proceedings of the IEEE Computer Society Conference on Computer Vision and Pattern Recognition*, June 2007.

[17] A. van der Schaaf and J. H. van Hateren, "Modelling the power spectra of natural images: statistics and information," *Vision Research*, vol. 36, pp. 2759–2770, 1996.

[18] M. S. Langer, "Large-scale failures of $f^{-\alpha}$ scaling in natural image spectra," *Journal of the Optical Society of America A*, vol. 17, no. 1, pp. 28–33, 2000.

[19] N. K. Bose, U. Srinivas, and R. L. Culver, "Wavelength diversity based infrared super-resolution and condition-based maintenance," *Insight*, vol. 50, no. 8, pp. 423–428, August 2008.

METODA REDUKCJI NADMIAROWOŚCI W STRUMIENIU DANYCH SEKWENCJI OBRAZÓW

Streszczenie

Sekwencje obrazów zawierają w sposób naturalny dużo strukturalnych powiązań (korelacji), co wiąże się ze znaczną nadmiarowością zawartych w nich informacji. Dla szybkiego przetwarzania i transmisji danych cyfrowych o takich sekwencjach konieczna jest redukcja w nich tych zbytecznych nadmiarowości. W artykule została zaproponowana i dogłębnie przebadana metoda służąca temu celowi. Jest ona, jak pokazano, efektywna. Od strony teoretycznej bazuje na zaproponowanych ulepszeniach, w wielu aspektach, technik dotychczas stosowanych.

Słowa kluczowe: metody redukcji nadmiarowości w strumieniu danych sekwencji obrazów